INFLUENCE OF HYDRAULIC RESISTANCE ON FLOW FEATURES IN AN OPEN CHANNEL CONFLUENCE

STÉPHAN CREËLLE(1), TOM DE MULDER(1), LAURENT SCHINDFESSEL(1) & TOMAS VAN OYEN(1)

(1) *Hydraulics Laboratory, Department of Civil Engineering, Ghent University, Ghent, Belgium, stephan.creelle@ugent.be*

Abstract

A numerical model based on the 3D shallow water equations is set up for a 90° angle open channel confluence. The model is first calibrated and validated using experimental data by (Shumate, 1998). Then a series of numerical simulations is carried out, systematically increasing the friction coefficient, in order to investigate the impact of hydraulic resistance on the flow features in an open channel confluence. The properties of the separation zone (width and length) are found to be substantially altered by the hydraulic resistance. The hydrodynamic processes are analysed zooming in onto lateral momentum fluxes.

Keywords: open channel confluence; hydrodynamics; bed roughness; numerical model; 3D shallow water equations

1. Introduction

The flow patterns at confluences of open channels and rivers have since long been studied intensively, in order to comprehend a variety of associated phenomena which are of great practical interest: upstream water level elevations, downstream mixing properties, erosion-sedimentation, local heterogeneities and ecohabitats, etc.

Through an effective blend of laboratory work, field studies and numerical modelling, it is well-known by now that the hydrodynamics of open channel confluences involves a number of distinct flow features, as sketched in Figure 1. Key variables to understand the confluence hydrodynamics are the ratio of incoming channel discharges, the junction angle, the channel depth to width ratio and the (possible) bed discordance.

As far as laboratory work in schematized confluences is concerned, one should be aware that most experiments have been performed in flumes with (relatively) smooth walls (Taylor, 1944; Hsu *et al*, 1998). Yet, the hydraulic resistance of confluences can exhibit a large variation, e.g. due to increased bed and bank roughness, or the occurrence of vegetation.

The objective of this paper is to assess the impact of increased bed friction on the flow features of a schematized open channel confluence. To this end, a numerical model is set up for a 90° angle confluence. In a first part, we calibrate and validate the model with the laboratory experiments conducted by Shumate (1998) in a smooth confluence flume. Thereafter, a parametric numerical study on the impact of the bed friction is presented. The focus of the analysis lies on the variation of the separation zone and associated lateral momentum fluxes.

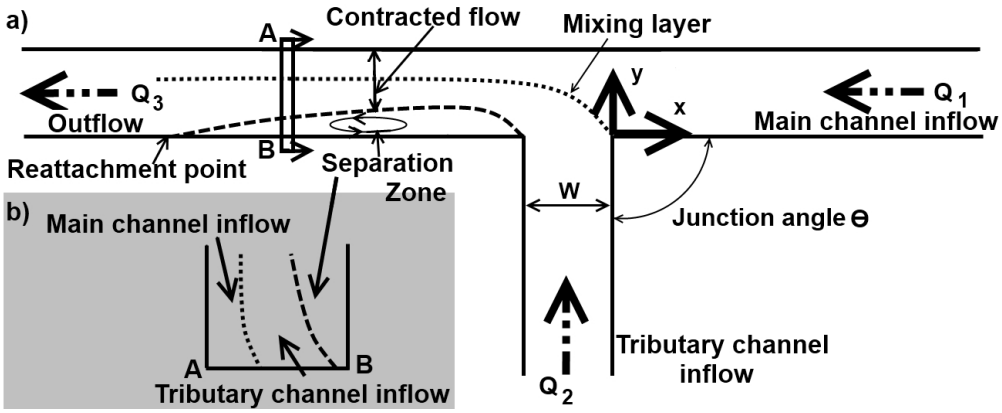

Figure 1: Sketch of open channel confluence and important flow features
a) plan view, b) cross-section

2. Confluence configuration

The configuration chosen for the numerical investigation in this paper is based on the laboratory flume experiments by Shumate (1998): an asymmetric confluence with a tributary channel and a main channel joining at an angle θ of 90° (see Figure 1). Both channels have a rectangular cross-section with equal width W. The fixed, horizontal beds of both channels are concordant.

A Cartesian coordinate system (x, y, z) is introduced. The horizontal x- and y-axes represent the streamwise and cross-stream directions, respectively. As shown in Figure 1, the origin of the coordinate system is at the upstream corner of the junction. Note that the x-axis is pointing in the upstream direction of the main channel. Hence, cross sections of the main channel downstream of the upstream junction corner will have negative values. The y-axis is pointing in the downstream direction of the tributary channel, and the z-axis points vertically upwards with origin at the bed level of the channels. The velocity components along the x-, y- and z-axes are denoted as u, v and w.

In this paper, the following notation convention is adopted: lowercase symbols (e.g. u) denote point values, an overbar (e.g. $\overline{u}$) corresponds to depth-averaged values and uppercase symbols (e.g. U) refer to values averaged over both depth and width (i.e. cross-sectionally averaged values). Furthermore, the results will be presented in non-dimensional form using W and U_o as length and velocity scales, respectively. The latter represents the cross-sectionally averaged tailwater velocity in the downstream section of the laboratory experiments.

Note that in Figure 1, section numbers are introduced to refer to the main channel inflow (section 1), the tributary channel inflow (section 2) and the main channel outflow (section 3). Hence, the discharges in those sections are denoted as Q_1, Q_2 and $Q_3 (= Q_1 + Q_2)$, respectively.

3. Setup and validation of numerical model

The open-source software suite Delft3D (Anonymous, 2011) is used to set up a model, based on the 3D shallow water equations, supplemented with a standard k-ε model and the so-called HLES model to describe the vertical resp. horizontal exchange of momentum due to turbulence. To parameterize the bottom shear stress, a quadratic friction law is used:

$$\tau_b = \rho c_f |u_b| u_b \quad [1]$$

where u_b denotes the near-bed velocity in the lowest layer of the model and c_f is the friction coefficient. The latter is imposed indirectly in Delft3D, by specifying a corresponding Manning coefficient.

Grid spacing is equidistant in the x- and y-direction, with a cell size of 0.035 m. This leads to 9880 cells for the main channel and 2860 cells in the side branch. Vertically, the water column is divided into 20 equidistant sigma-layers, yielding a layer thickness in the order of 0.02 m.

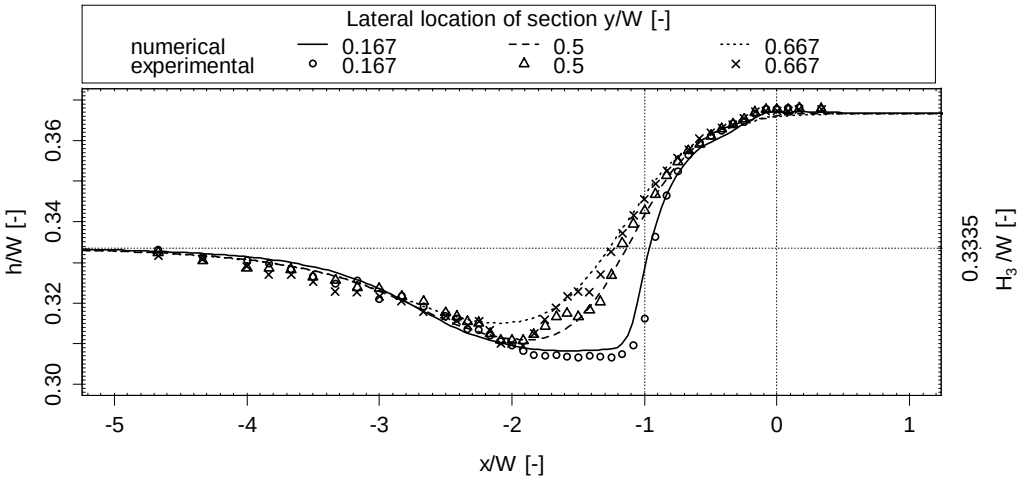

Figure 2: Comparison of measured (symbols) and modelled (lines) water depths along three streamwise transects.

The numerical model is calibrated, using c_f as calibration parameter, with respect to the laboratory measurements presented by Shumate (1998) in which the discharge ratio $q = Q_1/Q_3$ is set equal to 0.250. Figure 2 presents a comparison of the free surface elevation h observed in the laboratory experiments and the numerical model with a fitted value of c_f equal to 0.0026. Overall, a satisfactory agreement is obtained.

In Figure 3, the depth-averaged streamwise (left) and cross-stream (right) velocities obtained by the numerical model are compared with the measurements reported by Shumate (1998). Results show reasonable agreement of the model with the measurements. Yet, as indicated in the left figure, close to the wall the return flow (positive $\bar{u}$-values) in the separation zone is overestimated. This is due to the free slip boundary condition at the vertical walls in the numerical model. The cross-stream velocity component appears to be slightly underestimated by the model, however, the correct trend and shape is found. Overall, the model agreement is

reasonable. Validation runs (i.e. with the calibrated value of c_f = 0.0026), for two other cases, q=0.500 and q=0.750, exhibit a similar agreement of model results. These observations suggest that the numerical model can be used as a tool to perform the parametric study in the subsequent paragraphs.

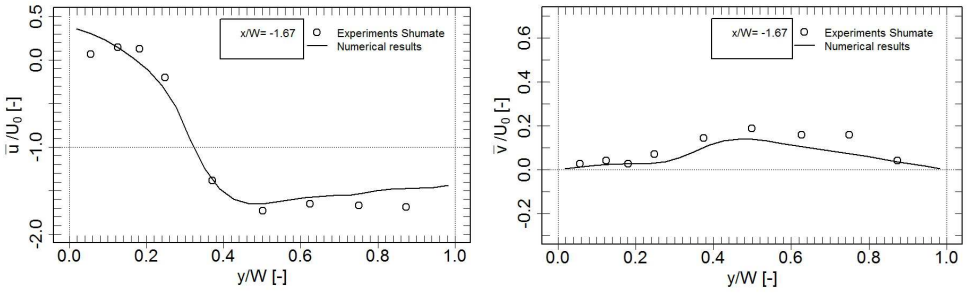

Figure 3: Comparison of the depth-averaged streamwise (left) and cross-stream (right) velocities obtained bythe numerical model to experimental values.

4. Results

In order to assess the impact of the hydraulic resistance, a series of simulations are performed considering different values of the friction coefficient; i.e. c_f = 0.008, 0.022, 0.114, 0.390, 0.976 and 1.970. Physically, the extremes of these values correspond to very smooth material (e.g. glass) and natural streams with a rough bed, respectively. The value of q is held constant at 0.250 in these simulations. In the following, first the impact on the free surface elevation and the characteristics of the separation zone is presented. Thereafter, we discuss the influence of c_f on the lateral and streamwise momentum fluxes, following the framework introduced by Rhoads and Sukhodolov (2008).

4.1 Water depths

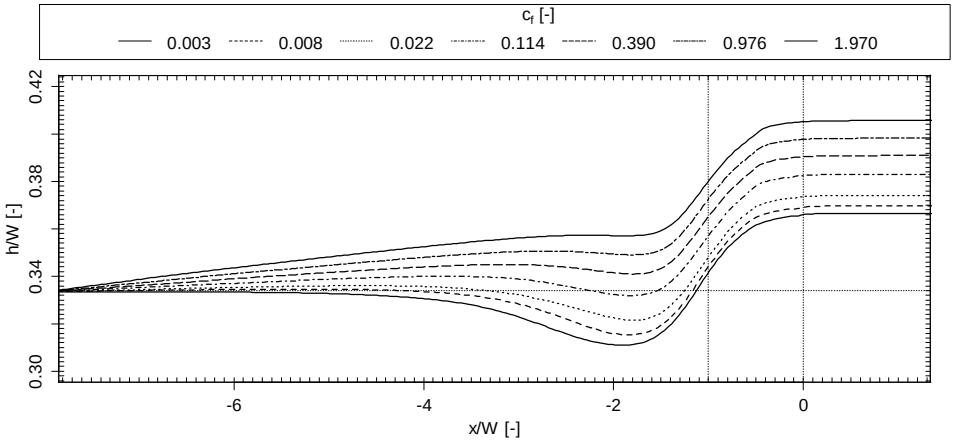

Figure 4: Longitudinal profiles of the water depth at y/W [-]=0.5 for different friction coefficients

Figure 4 shows the variation of the longitudinal profile of the water depth at the centerline of the main channel as a function of the friction coefficient. As expected, the water level elevation in the main channel increases with increasing bed roughness. Moreover, the local depression of the water surface immediately downstream of the confluence becomes less pronounced with increasing resistance, and the associated position of the local minimum water level shifts in the upstream direction.

4.2 Separation zone

At the downstream corner of the junction, the flow separates and gives rise to a zone with recirculating flow that does not contribute to the net downstream flow rate. To evaluate the local width y_s of this zone (in a given cross-section $x/W \leq -1$), we pragmatically compute the location where the integral of the depth-averaged downstream velocity along the cross-stream direction equals zero:

$$\int_0^{y_s} \int_0^{h} u \, dz dy = 0. \qquad [2]$$

Starting from a zero value at the separation point, y_s increases in downstream direction to a maximum value - i.e. the width W_s of the separation zone - and finally decreases again till a zero value is reached at the reattachment point. The length of the separation zone L_s is then defined as the distance between the separation and reattachment points. Note that in this simple approach, the dimensions of the separation zone are uniform over the water depth, which would turn out to be not fully correct if tracers were used to delineate the separation zone (Best and Reid, 1984).

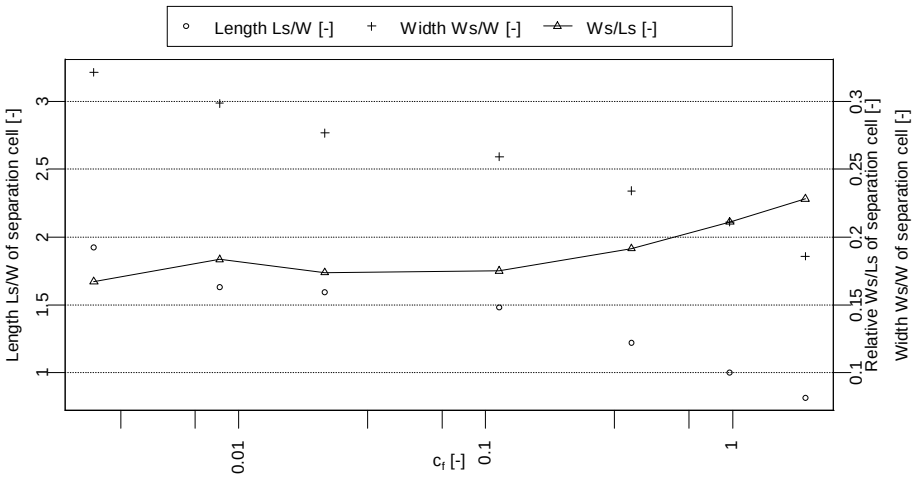

Figure 5: Dimensions of the separation zone as a function of the friction coefficient

The results of the numerical simulations in Figure 5 clearly show that both the length and the width of the separation zone decrease when the friction coefficient increases, whereas the ratio of width to length increases with increasing resistance. One should be aware, however, that accurate prediction of the separation zone dimensions (in particular its length) by means of a

RANS model, is not straightforward (Đorđević,2012). Yet, it is reassuring that the numerically predicted ratio W_s/L_s for c_f=0.003 (i.e. a value representative for smooth flume experiments) is well within the empirical range found by Best and Reid (1984).

4.3 Momentum flux

In order to facilitate the analysis of the influence of the hydraulic resistance on the numerically predicted (3D) flow fields at the confluence, we consider the depth-averaged (2D), steady state momentum equation in the streamwise direction:

$$\underbrace{\frac{\partial \bar{m}}{\partial x}}_{I} + \underbrace{\frac{\partial \rho h \overline{\bar{u}\bar{v}}}{\partial y}}_{II} + \underbrace{\frac{\partial \rho h \overline{(u-\bar{u})(v-\bar{v})}}{\partial y}}_{III} = -\rho g\, h\, \frac{\partial h}{\partial x} - \underbrace{\overline{\rho c_f |u_b| u_b}}_{IV} - \overline{T_{xx}} - \overline{T_{xy}}, \qquad [3]$$

with $\bar{m}$ the depth-integrated streamwise momentum flux (per unit width of the cross-section):

$$\bar{m} = \int_0^h m\ dz = \int_0^h \rho u^2\ dz, \qquad [4]$$

Note that the streamwise momentum flux integrated over the cross-section is given by αM, where $M = \rho U^2 WH$ and α denotes the momentum correction coefficient:

$$\alpha = \frac{\int_0^W \int_0^h m\ dzdy}{M} = \frac{\int_0^W \bar{m}\, dy}{M} = \frac{\int_0^W \int_0^h \rho u^2\ dzdy}{M}. \qquad [5]$$

For a uniform velocity profile, $\alpha = 1$, while α increases with the degree of non-uniformity.

4.3.1 Streamwise momentum flux

Figure 6A provides a contourplot of the values of $\bar{u}/U_o$, i.e. the dimensionless depth-averaged streamwise velocity, for the minimum and maximum value of the considered friction coefficients. The plots illustrate that the flow field is significantly distinct under both conditions. First, it is apparent that the maximum magnitude of the streamwise velocity reduces for higher values of the friction coefficient and, in this case, the area delineated by the peak-velocity isoline is also smaller. A similar observation (not visible in Figure 6A) can be made for the maximum velocity in the separation zone (i.e. the region with positive values of $\bar{u}/U_o$), resulting in stronger lateral gradients of the streamwise velocity component.

The obtained results can be understood as follows. Similar to flow in bends, the bottom friction facilitates the diversion of the lateral inflowing discharge. Hence, the width of the separation zone decreases for larger values of c_f. This corresponds to a larger portion of the cross-section being available to the downstream discharge, resulting in lower velocities.

Figure 6A additionally shows that increasing bed friction tends to intensify the uniformization of depth-averaged velocities. This is also illustrated in Figure 6B, which plots the value of α versus x/W for both values of the friction coefficient. In fact, it is found that α levels off faster (i.e. at a smaller distance downstream of the junction), in case of the higher friction coefficient. Note that the value of α at the downstream section 3, is higher in case of c_f= 1.970. This is due to the shape of the velocity profile over the depth deviating more from its depth-averaged value in case of higher friction coefficients.

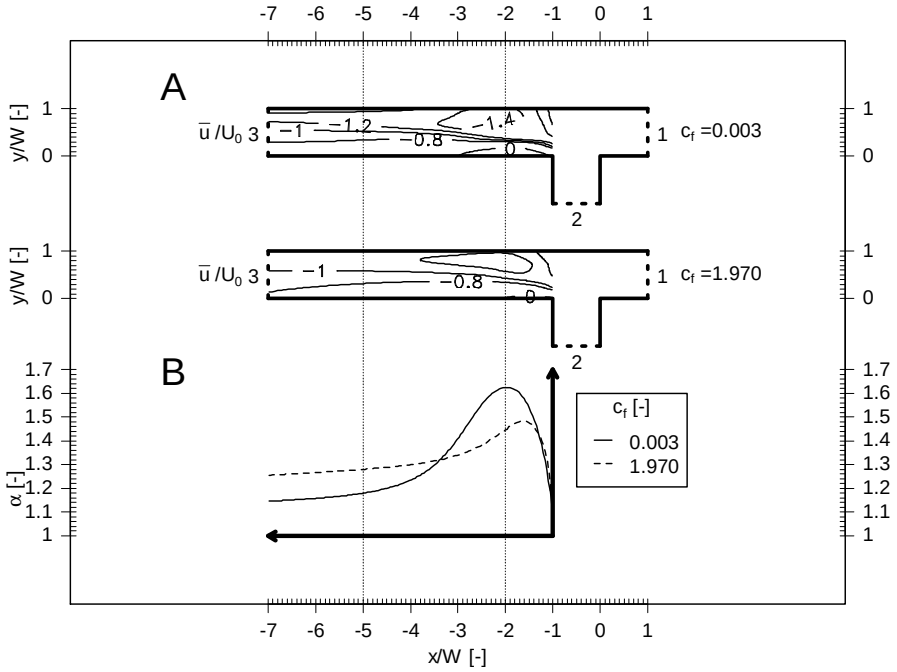

Figure 6: A) Contourplot of $\bar{u}/U_o$ for different values of the friction coefficient, B) Momentum correction coefficient α plotted as function of the x-direction

4.3.2 *Lateral momentum flux*

The previous section has discussed the downstream evolution of the streamwise momentum flux, shedding a light on term I in equation [3]. In the following, the impact of the hydraulic resistance on the lateral momentum fluxes is investigated. Term II in equation [3] represents the lateral transport of momentum by depth-averaged flow, while term III accounts for the lateral transport of momentum due to secondary structures in the flow. The aforementioned terms are plotted in Figure 7 (II: dashed line, III: full line). For reference purposes, the amplitude of the contribution due to bottom shear stress , i.e. term IV in equation [3], is also presented (IV: dotted line).

For the case of the low friction coefficient, the lateral momentum transport by depth-averaged flow (term II), exhibits pronounced positive and negative peaks at the section $x/W = -2$ (Figure 7A). These peaks coincide with the location of strong gradients in the depth-averaged velocity components $\bar{u}$ and $\bar{v}$, caused by the presence of the separation zone. The strong positive peak at $y/W = 0.3$ reduces the streamwise momentum deficit causing the recirculation zone. This goes along with a local streamwise momentum decrease, due to lateral transport of streamwise momentum from the region of $y/W = 0.5$. These strong peaks have vanished in section $x/W = -5$ (Figure 7C), where a more uniform positive contribution is observed in the range $y/W = 0$ to 0.5. This is associated with transporting streamwise momentum from the high momentum zone at $y/W = 0.65$.

For the high friction case (Figure 7B) a strong peak in term II is absent at the section $x/W = -2$,

indicating that gradients of velocities seem to be smaller. This is indeed confirmed by Figure 5, from which a separation zone length shorter than W can be read, i.e. $x/W = -2$ is downstream of the reattachment point.

For the lateral momentum transport by secondary structures (term III), a first observation from Figure 7 is that the magnitude is in the same order as the one of term II. This conclusion does not seem to agree with the one made by Rhoads and Sukhodolov (2008) based upon measurements made in a natural river confluence. This might be due to various causes, such as the strongly schematized geometry considered in this paper, the higher relative momentum contribution by the lateral channel, and the location of the cross-sections under consideration being more downstream of the junction. The latter cause indeed seems plausible, since the contribution of term II is an order of magnitude larger than the one of term III in the zone between $x/W = 0$ and $x/W = -1$, an observation in line with the one of Rhoads and Sukhodolov (2008).

The most important effect of higher values of the friction coefficient on term III is found to be located near the region of highest velocities (Figure 6A), hence associated with highest momentum content. While at low friction the secondary structures help redistributing the momentum in the lateral direction, at high friction these structures have a positive value in the region of high momentum. (An indication for this follows from a comparison of Figure 8B with 8D, where indeed an increase in the highest magnitudes of the streamwise velocity is observed.)

To further clarify the conclusions drawn from Figure 7, additional plots of velocity components in different cross-section are provided in Figure 8. In this figure, contourplots of u/U_o are plotted for low (left figures) and high (right figures) values of the friction coefficient. In addition, vector plots are provided to describe the velocity in the $y-z$ plane, indicating the three-dimensional circulation pattern.

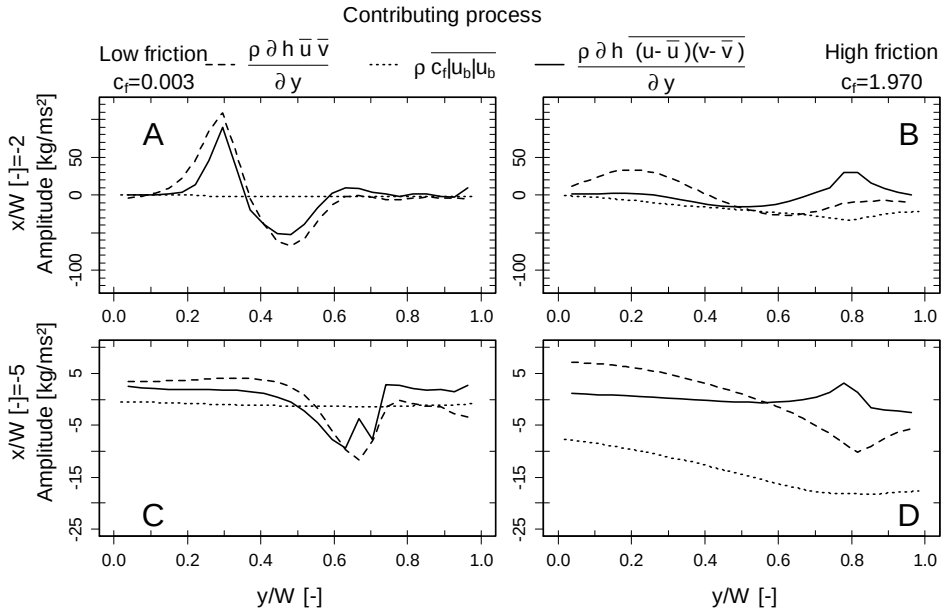

Figure 7: Amplitude profiles of the different processes of lateral momentum transport

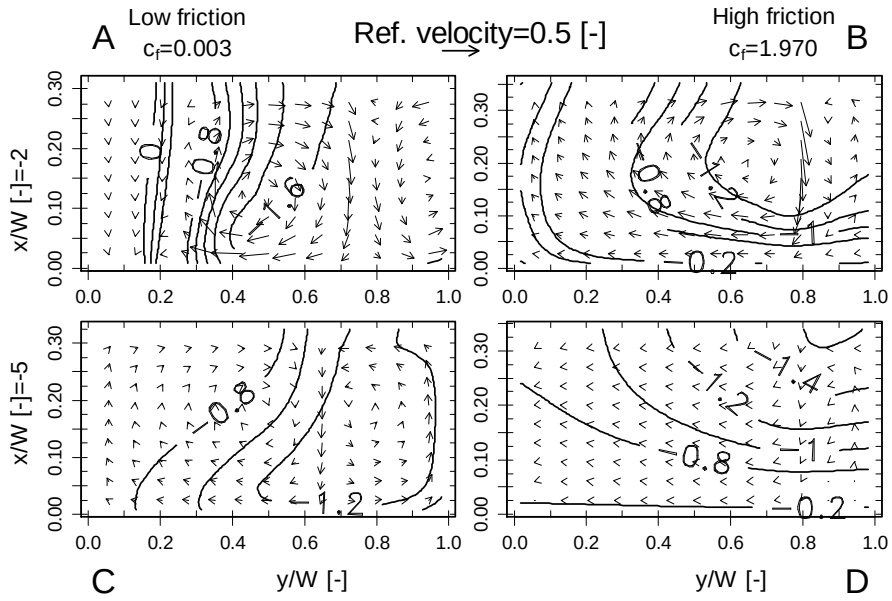

Figure 8: Velocity components in different cross-sections. Isolines: streamwise component u/U_o
Vectors: velocities in the y-z plane

5. Conclusions

In this paper, the impact of increased bed friction on the flow features of a schematized open channel confluence has been assessed by means of a numerical model.

The parametric study has revealed that flow features significantly alter when increasing the quadratic friction coefficient . Besides increased water level elevations over the confluence, bed friction also reduces the dimensions of the separation zone immediately downstream of the junction. Additionally, flow velocity profiles are strongly affected. E.g. the downstream evolution towards fully developed flow is intensified due to bed friction. The friction-dependent contribution of the lateral momentum fluxes in this redistribution process has been highlighted.

Taking into account that most laboratory work on schematized confluences so far has been performed in smooth walled flumes, the conclusions of this paper suggest that further research is needed in experimental flumes with increased bed friction. Whether other types of hydraulic resistance (Yen, 2002), like e.g. side wall roughness or vegetation, also have a pronounced effect on flow features in confluences cannot be concluded from this paper, but is worth investigating.

Finally it should be emphasized that the water depth to channel width ratio in the considered flow configuration is relatively high. The question then arises, how the conclusions of this work will change for more shallow flows, which are known to exhibit distinct flow features (Jirka and Uijttewaal, 2004).

Acknowledgements

The first author is Ph.D. fellow of the Special Research Fund (BOF) of Ghent University. The third and fourth authors are Ph.D. fellow and Postdoctoral fellow of the Fund of Scientific Research – Flanders (Belgium) (FWO-Vlaanderen).

References

Anonymous, 2011. 'Delft3D-FLOW: User Manual', Deltares, Delft , pp. 672.

Best, J.L. and Reid, I., 1984. 'Separation zone at open channel junctions', *Journal of Hydraulic Engineering*, Vol. 110, 11, 1588-1594.

Đorđević, D., 2012. 'Application of 3D numerical models in confluence hydrodynamics modelling', *XIX International Conference on Water Resources,* Champaign (Illinois), June 2012.

Hsu, C.C. ,Wu, F.S and Lee, W.J. , 1998. 'Flow at 90° Equal-Width Open-Channel Junction', *Journal of Hydraulic Engineering*, Vol. 124, 2, 186-191.

Jirka, G. H., and Uijttewaal, W. S., 2004. 'Shallow flows: a definition'. *Shallow flows*, Taylor & Francis Group, ISBN 9058097005, 3-11.

Rhoads, B.L. and Sukhodolov, A., 2008. 'Lateral momentum flux and the spatial evolution of flow within a confluence mixing interface', *Water Resources Research*, Vol. 44, 8, W08440.

Shumate, E.D., 1998. 'Experimental description of flow at an open-channel junction', Unpublished Master thesis. Univ. of Iowa, Iowa, pp. 150.

Taylor, E.H., 1945. 'Flow characteristics at rectangular open-channel junctions'. *Trans ASCE*. Vol.107, 893–912.

Yen, B., 2002. 'Open Channel Flow Resistance', *Journal of Hydraulic Engineering*. Vol. 128, 1, 20-39.